

Measurement of Electron Trapping in the CESR Storage Ring

M.G. Billing, J. Conway, E.E. Cowan, J.A. Crittenden,* W. Hartung,
J. Lanzoni, Y. Li, C.S. Shill, J.P. Sikora, and K.G. Sonnad
CLASSE, Cornell University, Ithaca, NY 14850, USA

The buildup of low-energy electrons has been shown to affect the performance of a wide variety of particle accelerators. Electron clouds can cause instabilities and emittance growth and can also result in excess heat load on cryogenic systems. Of particular concern is the persistence of the cloud between beam bunch passages, which can impose limitations on the stability of operation at high total beam current. We have obtained measurements of long-lived electron clouds trapped in the field of a quadrupole magnet in a positron storage ring, with lifetimes much longer than the revolution period. Based on modeling, we estimate that about 7% of the electrons in the cloud generated by a 20-bunch train of 5.3 GeV positrons with 16-ns spacing and 1.3×10^{11} population survive longer than $2.3 \mu\text{s}$ in a quadrupole field of gradient 7.4 T/m. We have observed a non-monotonic dependence on the spacing of the bunches, indicating a beam-induced multipacting effect. A witness bunch provides a direct measurement of the trapped cloud density. The witness bunch is also observed to clear the cloud, demonstrating its effectiveness as a mitigation technique.

I. INTRODUCTION

Electron cloud buildup has been observed in many accelerators since the 1960s [1], and was an important factor in the operation of the positron storage rings at KEKB in Japan [2] and PEP-II in the U.S. [3], resulting in the installation of solenoidal magnetic field windings on the beam-pipes. Trapping of electrons oscillating around a 70-m-long proton bunch in the LANL PSR storage ring has been reported in Ref. [4]. Measurements of the time dependence of electron cloud buildup have been reported at LBNL [5], where the electrons were observed to be trapped in the fields of an ion beam and accelerator elements. Simulations were used to study electron trapping in quadrupole and sextupole magnets for the parameters of the KEKB positron ring [6], as well as for the Cornell Electron Storage Ring (CESR) and the positron damping ring of the International Linear Collider [7]. The Large Hadron Collider (LHC) upgrade is contingent on reducing the bunch spacing to 25 ns [8], where electron cloud effects are severe enough that they have been used for scrubbing runs [9]. Cloud mitigation efforts are under study, including application of carbon coatings to the dipole magnet vacuum chambers in the SPS [10]. Estimates of long-lived electron cloud buildup at the LHC and consequences for vacuum chamber heat load have been presented in Ref. [11]. More recently, heat load in the final-focus quadrupoles of the LHC has been attributed to electron cloud buildup [12]. The design for the SuperKEKB collider to be commissioned in 2015 has incorporated an extensive set of electron cloud mitigation techniques [13]. Since the solenoidal windings employed in the field-free regions of the ring cannot be used in the quadrupole magnets for field quality reasons, cloud mitigation methods are limited to TiN coatings and antechambers.

We report here on the measurement of electron trapping over an entire $2.5 \mu\text{s}$ CESR beam revolution period resulting from electron cloud buildup in a quadrupole magnet. Since the trapping mechanism is not contingent upon the beam potential, as was the case at the PSR, beam-free intervals in the ring are ineffective at clearing the electrons.

A principal goal of the Cornell Electron Storage Ring Test Accelerator program [14] is to investigate performance limitations in future high-energy low-emittance rings. These studies include measurements of electron cloud buildup caused by synchrotron-radiation-induced photoemission on the surface of the vacuum chamber. The CESR ring stores positron and electron beams of energy 1.8 GeV to 5.3 GeV arranged in bunches spaced in intervals of 4 or 14 ns with bunch populations ranging up to 1.6×10^{11} . A variety of detectors sensitive to cloud electrons incident on the vacuum chamber wall have been commissioned [15–17]. Recently, we developed a novel method for time-resolved measurements of electron cloud buildup in a quadrupole magnet.

II. TIME-RESOLVING ELECTRON DETECTOR

Time-resolving electron detectors have provided detailed information on local cloud formation, allowing the independent characterization of photoelectron and secondary electron production mechanisms [18, 19]. We have installed a shielded detector in a circular stainless steel vacuum chamber of inner diameter 95.5 mm inside a 60-cm-long quadrupole magnet, as shown in Fig. 1a. The detector is located in front of a magnet pole, as shown in Fig. 1b. Electrons are collected on the 6-mm-wide copper trace (Fig. 1c) which tapers to a transmission line using the grounded copper on the other side of the 0.12-mm-thick Kapton sheet. The total length of the trace including the 6-mm-wide, 102-mm-long rectangular central region is 907 mm. The pattern of 5×60 parallel holes 0.8 mm in diameter shown in Fig. 1d allows passage of

* crittenden@cornell.edu

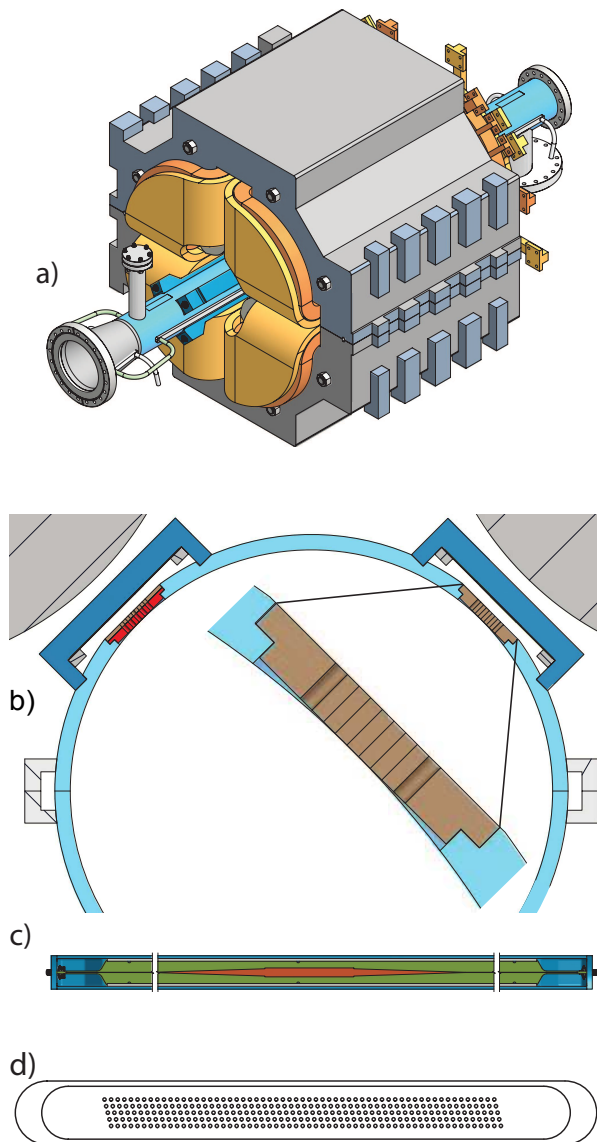


FIG. 1. a) Vacuum chamber equipped with electron detectors in the quadrupole magnet. b) Arrangement of two detectors in front of the magnet poles as seen from the positron arrival direction. c) Geometry of the copper electrode biased at 50 V to collect electrons entering through the pattern of holes in the beam-pipe shown in d). The rectangular region of the collector and the pattern of holes are each about 10 cm long.

cloud electrons through the beam-pipe to the collector. The chosen hole diameter gives a depth-to-diameter ratio of 3:1 in order to shield the detector from the RF power radiated during the passage of the 18-mm-long positron bunches [20]. The hole pattern is 7.1 mm wide and 94.4 mm long. Figure 2 shows a schematic view of the beam-pipe, hole pattern and detector arrangement.

The collector is biased at +50 V relative to the vacuum chamber in order to prevent secondary electrons from leaving the collector surface. The AC-coupled front-end readout electronics consists of two Mini-Circuits ZFL-500 broadband amplifiers with 50 Ω input impedance

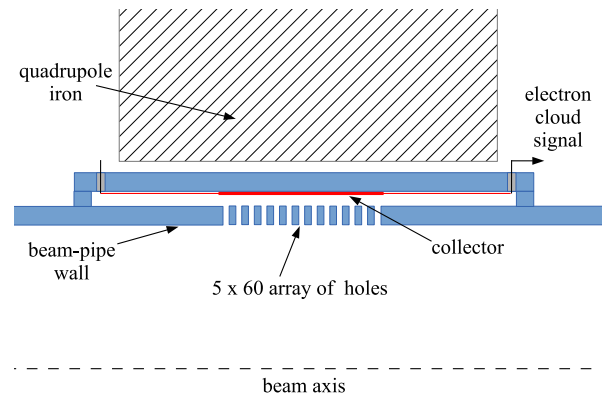


FIG. 2. Schematic cross section of the electron detector, which is located near the longitudinal center of the quadrupole magnet. The holes in the beam-pipe wall allow cloud electrons to reach the collector.

and a total gain of 40 dB. Oscilloscope traces are digitized to 8-bit accuracy in 1000 time bins, typically 0.5 or 1.0 ns wide, averaging over 8000 beam-synchronous triggers. The direct beam-induced signal from the residual transmission of high-frequency RF power through the shielding holes results in a damped ringing in the raw oscilloscope signals. All signals depicted in the figures below show the result of applying a 13-MHz low-pass digital post-processing filter which suppresses this noise by an order of magnitude.

Figure 3 shows the filtered signals for 10- and 20-bunch trains of 5.3 GeV positrons. The bunches have rms sizes of 1.8 mm horizontally and 0.08 mm vertically. The average bunch population is 1.3×10^{11} . The bunch spacing is 14 ns and the bunch-to-bunch population is uniform to a few percent. The quadrupole field gradient is 7.4 T/m, horizontally focusing.

The larger signal during the first 10 bunches of the 20-bunch train relative to that for the 10-bunch train shows the presence of cloud prior to the arrival of the

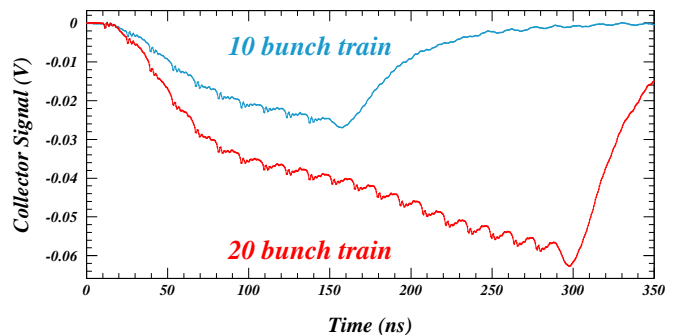


FIG. 3. Electron detector signals recorded for 10- and 20-bunch trains of 5.3 GeV positrons for an average bunch population of 1.3×10^{11} . The enhanced signal during the first 10 bunches of a 20-bunch train relative to that for the 10-bunch train shows that electrons were trapped during the entire 2.3 μ s interval prior to the return of the bunch train.

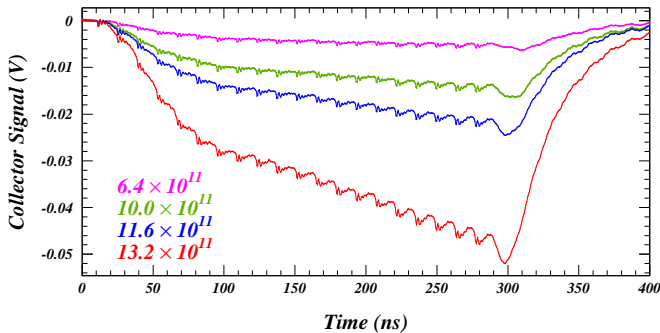


FIG. 4. Dependence of the signals on bunch population for 20-bunch trains with 14 ns spacing. The dependence is strongly nonlinear, the signal amplitude increasing by an order of magnitude for a factor of two increase in bunch population.

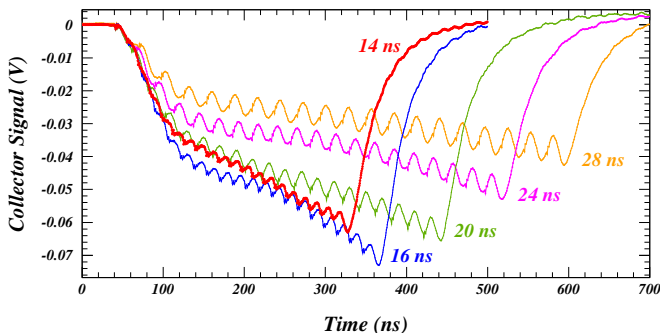


FIG. 5. Comparison of signals obtained from 20-bunch trains with spacing 14, 16, 20, 24 and 28 ns. The increase in signal for the 16-ns spacing relative to the 14-ns spacing shows that the beam-induced multipacting enhances long-term cloud electron trapping.

train. One can deduce that electrons remain trapped at least as long as the $2.3 \mu\text{s}$ beam-free interval prior to the return of the bunch train. The decrease in cloud buildup rate following the first 6 bunches indicates that a subset of trapped electrons which can contribute signal has become depleted at that time. In spite of this clearing of the trapped reservoir of electrons, the signal does not return to the level of the 10-bunch signal, showing that the additional cloud seeded by the long-term trapping is self-sustaining. The signal depends strongly on the bunch population, decreasing by an order of magnitude as the bunch population decreases by a factor of two from 1.3×10^{11} to 6.4×10^{11} , as shown in Fig. 4.

The dependence of trapping on the bunch spacing is shown in Fig. 5 for a bunch population of about 1.3×10^{11} . The increase in the trapped signal as the bunch spacing is raised from 14 ns to 16 ns is the signature of the beam-induced multipacting enhancement investigated by Harkay and Rosenberg at the Advanced Photon Source [21].

We have investigated the effectiveness of an intermediate bunch as a mechanism for clearing the trapped cloud. Figure 6 shows the three signals obtained from 1) a 20-

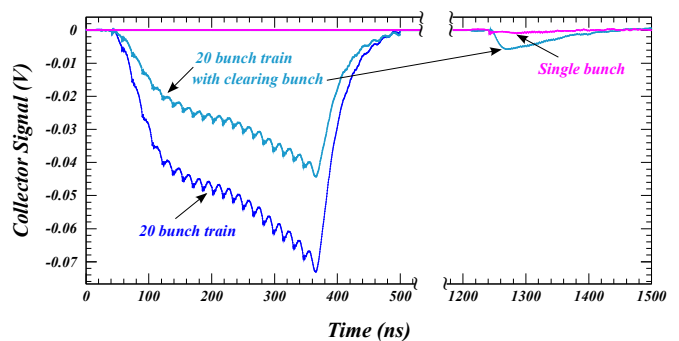


FIG. 6. Effect of an intermediate clearing bunch following about 900 ns after the end of a 20-bunch train for the case of 16-ns spacing. The difference in magnitude between the signals at 1250 ns is directly sensitive to the trapped electrons produced by the 20-bunch train.

bunch train, 2) a 20-bunch train with a clearing bunch following about 900 ns after the end of the train, and 3) a single bunch. The single-bunch signal is plotted to coincide with the signal from the clearing bunch for the purpose of comparison. The clearing bunch accelerates trapped cloud electrons into the detector, and thus provides direct evidence for the trapped cloud. In addition, the reduced signal from the 20-bunch train when the clearing bunch is present shows the effectiveness of such a mitigation technique. We verified that the clearing effectiveness is independent of the delay of the clearing bunch over a range of ± 500 ns. The full clearing effect was achieved when the clearing bunch population reached about 20% of the average population of the bunches in the train.

III. TRAPPING MECHANISM

The long-term trapping of electrons in nonuniform fields such as quadrupole fields can be understood in terms of an adiabatic magnetic moment μ given by

$$\mu = mv_{\perp}^2/2B, \quad (1)$$

where m is the mass of the electron, B is the magnetic field magnitude, and v_{\perp} is the velocity perpendicular to the magnetic field vector (see, for example, Ref. [22]). This quantity remains invariant as long as $dB/B \ll 1$ during the cyclotron motion, or equivalently,

$$\Gamma = |\nabla B|r_c/B \ll 1, \quad (2)$$

where r_c is the cyclotron radius. Combining the conditions of conservation of magnetic moment and conservation of energy, one can specify a “velocity-space loss cone” angle, Θ_{LC} , which defines the trapping condition. A particle moving from a region of lower field to a region of higher field reverses its path if the velocity components perpendicular and parallel to the magnetic field at

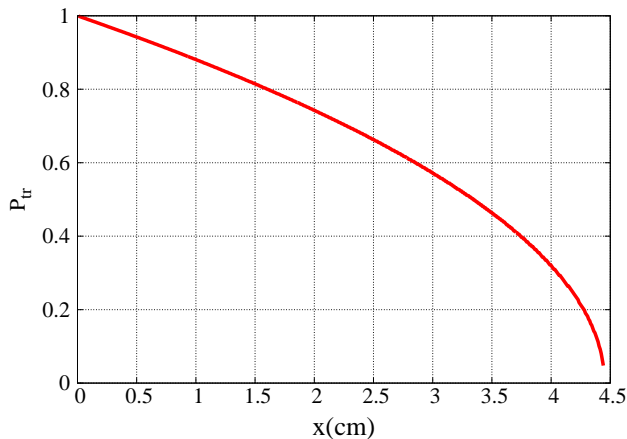


FIG. 7. Cosine of the loss-cone angle, P_{tr} , versus horizontal position in the mid-plane of the vacuum chamber. The trapping probability increases toward the center of the chamber as long as the adiabaticity condition is satisfied.

the starting position, denoted by v_{\perp}^{in} and $v_{\parallel}^{\text{in}}$ respectively, are related such that

$$v_{\parallel}^{\text{in}}/v_{\perp}^{\text{in}} \leq (B_{\text{bd}}/B_{\text{in}} - 1)^{1/2}. \quad (3)$$

Here B_{in} is the magnetic field magnitude at the start point, and B_{bd} is the magnitude along the field line at the boundary beyond which the particle is lost. If the above relationship is satisfied, the particle reaches a point where the parallel velocity goes to zero, and the particle reverses its path along the field line. In a quadrupole magnetic field, the trapped particle is confined between two such mirror points located along a field line symmetric about either the horizontal or the vertical axis. While the particle mirrors between the pair of points, it drifts in the longitudinal direction until it reaches the fringe region of the quadrupole, where it can escape [23]. This drift is caused by a nonzero gradient and curvature in the magnetic field, often referred to as the “grad B” and “curvature” drift respectively. For a 7.4 T/m field gradient, the longitudinal drift over the duration of one CESR beam revolution is significant only when the electron energy is of the order of 1 keV. The energy distribution obtained from the cloud build-up modeling described below indicate that less than 3% of the electrons have energies exceeding 1 keV.

The cosine of the loss cone angle represents the fractional solid angle in velocity space within which a particle remains confined. Thus, for a localized distribution of isotropic velocities, it represents the probability of confinement at that point. This quantity may be expressed as

$$P_{\text{tr}} = \cos \Theta_{\text{LC}} = (1 - B_{\text{in}}/B_{\text{bd}})^{1/2} \quad (4)$$

and is shown in Fig. 7 as a function of horizontal position x along the mid-plane of the vacuum chamber. The probability of confinement decreases with x , provided $\Gamma \ll 1$.

The adiabatic condition can be expressed as

$$\Gamma = \sqrt{2mE_{\perp}/e}/Kx^2 \ll 1, \quad (5)$$

where K is the quadrupole field gradient and E_{\perp} the kinetic energy corresponding to the velocity component perpendicular to the magnetic field. For electrons in a quadrupole with field gradient $K = 7.4$ T/m, Γ reduces to

$$\Gamma = 4.6 \times 10^{-3} \frac{\sqrt{E_{\perp}/\text{eV}}}{(x/\text{cm})^2}. \quad (6)$$

For comparison, the beam kick produced by a bunch carrying 1.3×10^{11} positrons on an electron at the vacuum chamber wall is 60 eV in the impulse approximation, easily satisfying the trapping condition. On the other hand, an electron with a horizontal momentum of 40 keV/c located 1 cm from the beam in the horizontal mid-plane is likely to hit the chamber wall.

IV. NUMERICAL MODELING OF ELECTRON CLOUD BUILDUP

We have employed a particle-in-cell, time-sliced cloud buildup modeling code [24] to improve our understanding of the electron trapping mechanism and the observed signals. The code includes simulation algorithms for photoelectron generation, macroparticle tracking in the 2D electrostatic fields of the beam and the cloud, and 3D tracking in a variety of ambient magnetic fields, as well as for a detailed model of the interaction of cloud electrons with the vacuum chamber surface [25].

The code has been supplemented with response functions for the CESR-TA time-resolving electron detectors [26]. As a function of incident angle and energy, a fraction of the macroparticle charge hitting the wall in the region of the detector contributes to the modeled signal. The fraction is derived from an analytic calculation of the hole acceptance for the case of a magnetic field parallel to the hole axis. For an arbitrary magnetic field strength, the acceptance of the holes is derived by relating the incident kinetic energy and angle to the cyclotron radius and the wall traversal time, i.e. the fractional number of cyclotron revolutions performed. Thus the acceptance at high field extends to grazing angles of incidence when the cyclotron radius is smaller than the hole radius.

The amplitude of the modeled signal was found to be very sensitive to the assumed secondary emission yield, increasing by an order of magnitude as the peak secondary yield was increased from 1.4 to 1.9. The measured signal amplitude was reproduced with values for the peak secondary yield and elastic yield of 1.4 and 0.5, respectively.

The model shows the signal to be generated predominantly by electrons originally produced on the field lines entering the detector, i.e. from a narrow surface region in

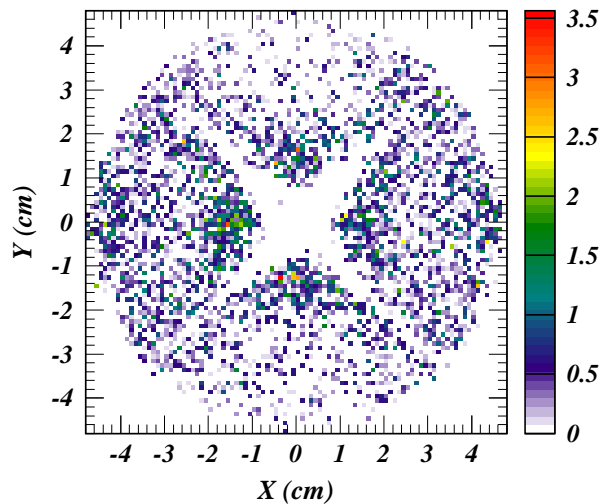


FIG. 8. The modeled transverse distribution of the trapped cloud shown at the end of the first beam revolution. The color scale ranges up to a maximum of 3.5×10^6 electrons/bin.

front of the diametrically opposed pole and from 4-mm-wide regions on the vacuum chamber surface in front of the other two poles extending from the middle of the pole toward the detector. These signal macroparticles spiral around field lines which pass within a few millimeters of the beam. The electrons which remain trapped during the $2.3 \mu\text{s}$ prior to the train arrival are cleared out during the first 6 of the 20 bunch passages, reabsorbed either in the detector or the vacuum chamber wall. The signal also shows, however, that the cloud development proceeds at the higher density level following the clearing, since it does not return to the level of the signal for a 10-bunch train. The trapping results in a sustained higher cloud density even after the trapped electrons have been removed. The peak density in the absence of the clearing bunch reaches $1.1 \times 10^{12} \text{ m}^{-3}$ after three turns, about 7% of which is trapped until the train returns. The clearing bunch reduces the trapped cloud density by about a factor of four.

The modeled transverse distribution of the cloud trapped in the quadrupole magnet is shown at a time immediately preceding the return of the train in Fig. 8.

The trapped electrons are concentrated in four quadrants near the beam outside of a central depletion zone of 2 cm radius, consistent with the trapping probability distribution shown in Fig. 7 and the non-adiabaticity in the central and diagonal regions. The median energy of the trapped electrons is about 50 eV.

V. SUMMARY

Our measurements with a time-resolving electron detector located in a quadrupole magnetic field have provided comparisons of signals from 10- and 20-bunch trains of positrons which show clear evidence for electron trapping during the entire $2.3 \mu\text{s}$ time interval prior to the return of the bunch train. Modeling tuned to the recorded signals indicates that approximately 7% of the cloud generated by a 5.3 GeV train of 20 bunches, each carrying 1.3×10^{11} positrons, remains trapped. The measurements show a non-monotonic dependence on bunch spacing indicative of beam-induced multipacting effects. The clearing effect of an intermediate bunch has been measured and successfully modeled, showing the trapped cloud can be reduced by a factor of four by such a clearing bunch. This characteristic of a quadrupole magnetic field to concentrate electrons near the beam raises concerns for storage rings with positively charged beams, since those electrons can be attracted into the beam. Measurements to quantify electron trapping in quadrupole magnets provide information useful for the development of simulation codes serving to predict electron cloud phenomena in future accelerators and to aid in the design of mitigation techniques.

VI. ACKNOWLEDGMENTS

We wish to thank Joe Calvey, Gerry Dugan, Miguel Furman and David Rubin for useful discussions. This work is supported by the US National Science Foundation contracts PHY-0734867, PHY-1002467, and PHY-1068662, by the US Department of Energy contract DE-FC02-08ER41538 and by the Japan/US Cooperation Program.

-
- [1] F. Zimmermann, “Electron-Cloud Effects in Past & Future Machines—Walk through 50 Years of Electron-Cloud Studies,” in *Proceedings of E-CLOUD 2012: Joint INFN-CERN-EuCARD-AccNet Workshop on Electron-Cloud Effects, La Biodola, Elba, Italy*, R. Cimino, G. Rumolo & F. Zimmermann, Eds., CERN, Geneva, Switzerland (2013), CERN-2013-002, p. 9–17.
- [2] K. Ohmi, “Beam-Photoelectron Interactions in Positron Storage Rings,” *Phys. Rev. Lett.* **75**, p. 1526–1529 (Aug. 1995).

- [3] M. A. Furman & G. R. Lambertson, “The Electron-Cloud Instability in PEP-II: An Update,” in *Proceedings of the 1997 Particle Accelerator Conference, Vancouver, BC, Canada*, IEEE (1997), p. 1617–1619.
- [4] R. J. Macek *et al.*, “Electron Cloud Generation and Trapping in a Quadrupole Magnet at the Los Alamos Proton Storage Ring,” *Phys. Rev. ST Accel. Beams* **11**, 010101 (Jan. 2008).
- [5] M. Kireeff Covo *et al.*, “Absolute Measurement of Electron-Cloud Density in a Positively Charged Particle Beam,” *Phys. Rev. Lett.* **97**, 054801 (Aug. 2006).

- [6] L. F. Wang *et al.*, “Photoelectron Trapping in Quadrupole and Sextupole Magnetic Fields,” *Phys. Rev. E* **66**, 036502 (Sep. 2002).
- [7] L. Wang & M. Pivi, “Trapping of Electron Cloud in ILC/CesrTA Quadrupole and Sextupole Magnets,” in *Proceedings of ELOUD 2010: 49th ICFA Advanced Beam Dynamics Workshop on Electron Cloud Physics*, Ithaca, NY, K. Smolenski, Ed., Cornell University, Ithaca, NY (2013), p. 167–172.
- [8] L. Rossi, “LHC Upgrade Plans: Options and Strategy,” in *Proceedings of the 2011 International Particle Accelerator Conference, San Sebastián, Spain*, EPS-AG (2011), p. 908–912.
- [9] G. Iadarola & G. Rumolo, “Electron Cloud in the CERN Accelerators (PS, SPS, LHC),” in *Proceedings of ELOUD 2012: Joint INFN-CERN-EuCARD-AccNet Workshop on Electron-Cloud Effects, La Biodola, Elba, Italy*, R. Cimino, G. Rumolo & F. Zimmermann, Eds., CERN, Geneva, Switzerland (2013), CERN-2013-002, p. 19–26.
- [10] C. Yin Vallgren *et al.*, “Performance of Carbon Coating for Mitigation of Electron Cloud in the SPS,” in *Proceedings of the 2011 International Particle Accelerator Conference, San Sebastián, Spain*, EPS-AG (2011), p. 1590–1592.
- [11] R. Cimino *et al.*, “Can Low-Energy Electrons Affect High-Energy Physics Accelerators?” *Phys. Rev. Lett.* **93**, 014801 (Jul. 2004).
- [12] K. Brodzinski & L. Tavian, “First Measurements of Beam-induced Heating on the LHC Cryogenic System,” Tech. Rep. CERN-ATS-2013-009, CERN, Geneva, Switzerland (Jan. 2013), presented at the International Cryogenic Engineering Conference/International Cryogenic Materials Conference, Fukuoka, Japan, May 2012.
- [13] Y. Suetsugu *et al.*, “Design and Construction of the SuperKEKB Vacuum System,” *J. Vac. Sci. Technol. A* **30**, 031602 (May 2012).
- [14] G. F. Dugan, M. A. Palmer & D. L. Rubin, “ILC Damping Rings R&D at CesrTA,” in *ICFA Beam Dynamics Newsletter*, J. Urakawa, Ed., International Committee on Future Accelerators, No. 50, p. 11–33 (Dec. 2009).
- [15] J. R. Calvey *et al.*, “Comparison of Electron Cloud Mitigating Coatings Using Retarding Field Analyzers,” *Nucl. Instrum. Methods Phys. Res.* **A760**, p. 86–97 (Oct. 2014).
- [16] J. R. Calvey *et al.*, “Measurement and Modeling of Electron Cloud in a Field Free Environment Using Retarding Field Analyzers,” *Phys. Rev. ST Accel. Beams* **17**, 061001 (Jun. 2014).
- [17] J. A. Crittenden *et al.*, “Modeling for Time-Resolved Retarding Field Analyzer Measurements of Electron Cloud Buildup at CesrTA,” in *IPAC2013: Proceedings of the 4th International Particle Accelerator Conference, Shanghai, China*, Z. Dai *et al.*, Eds., JACoW (2013), p. 846–848.
- [18] J. A. Crittenden *et al.*, “Shielded Button Electrodes for Time-Resolved Measurements of Electron Cloud Buildup,” *Nucl. Instrum. Methods Phys. Res.* **A749**, p. 42–46 (Jun. 2014).
- [19] J. A. Crittenden & J. P. Sikora, “Electron Cloud Buildup Characterization Using Shielded Pickup Measurements and Custom Modeling Code at CesrTA,” in *Proceedings of ELOUD 2012: Joint INFN-CERN-EuCARD-AccNet Workshop on Electron-Cloud Effects, La Biodola, Elba, Italy*, R. Cimino, G. Rumolo & F. Zimmermann, Eds., CERN, Geneva, Switzerland (2013), CERN-2013-002, p. 241–250.
- [20] M. Sands, “Energy Loss from Small Holes in the Vacuum Chamber,” Tech. Rep. PEP-253, SLAC, Stanford, CA (Sep. 1977).
- [21] K. C. Harkay & R. A. Rosenberg, “Properties of the Electron Cloud in a High-Energy Positron and Electron Storage Ring,” *Phys. Rev. ST Accel. Beams* **6**, 034402 (Mar. 2003).
- [22] R. J. Goldston & P. H. Rutherford, *Introduction to Plasma Physics*, Institute of Physics, Bristol (1995).
- [23] E. E. Cowan, K. G. Sonnad & S. Veitzer, “Trajectories of Low Energy Electrons in Particle Accelerator Magnetic Structures,” in *NA-PAC 2013: Proceedings of the 2013 North American Particle Accelerator Conference, Pasadena, CA*, T. Satogata, C. Petit-Jean-Genaz & V. Schaa, Eds., JACoW (2013), p. 475–477.
- [24] G. Rumolo & F. Zimmermann, “Electron Cloud Simulations: Beam Instabilities and Wakefields,” *Phys. Rev. ST Accel. Beams* **5**, 121002 (Dec. 2002).
- [25] M. A. Furman & M. T. F. Pivi, “Probabilistic Model for the Simulation of Secondary Electron Emission,” *Phys. Rev. ST Accel. Beams* **5**, 124404 (Dec. 2002).
- [26] J. A. Crittenden *et al.*, “Numerical Modeling for CESR-TA Measurements of Electron Cloud Buildup in a Quadrupole Magnet,” in *IPAC2014: Proceedings of the 5th International Particle Accelerator Conference, Dresden, Germany*, C. Petit-Jean-Genaz *et al.*, Eds., JACoW, Geneva, Switzerland (2014), p. 1632–1634.